Washington University in St. Louis

Washington University Open Scholarship

Mechanical Engineering and Materials Science Independent Study

Mechanical Engineering & Materials Science

12-20-2016

Continued study on finite element models of flagella

Gary Hu
Washington University in St. Louis

Philip V. Bayly
Washington University in St. Louis

Follow this and additional works at: https://openscholarship.wustl.edu/mems500

MEMS400 Independent Study Report

Continued study on finite element models of flagella

by
Gary Hu

Advisor: Professor Philip Bayly

Submitted in partial fulfillment of the requirements
for independent study Fall 2016

Department of Mechanical Engineering & Materials Science
Washington University in St. Louis

December, 2016

Abstract

In previous study, we developed finite element models of flagella that show wavelike oscillation above certain load threshold. However, these baseline models were highly simplified and had inevitable limitations. In the current study, inter-doublet components have been meshed with finer setting to give more accurate results, multibody dynamics (translational joints) has introduced to allow more deflection, and inter-doublet materials have included viscoelasticity. Nondimensional waveform equations have been developed to find parameter values that allow larger deflection and frequencies close to actual cilia and flagella.

Table of Contents

1   Introduction

Cilia and flagella are slender organelles that show propulsive, wavelike oscillations to propel cell and move fluid. Previous work (**1**) has been done to develop finite element models of flagella using a commercial software package called ABAQUS (Dassault Systemes). In previous models (**Fig. 1**), flagella model was composed entirely of linear, elastic beam elements in ABAQUS, and all beams were welded. On each pair of coupled beams, opposing, distributed axial loads and counter-moments were applied to represent dynein loads, such that above certain threshold, the flagella model would show wavelike oscillation (**Fig. 2**) due to dynamic instability.
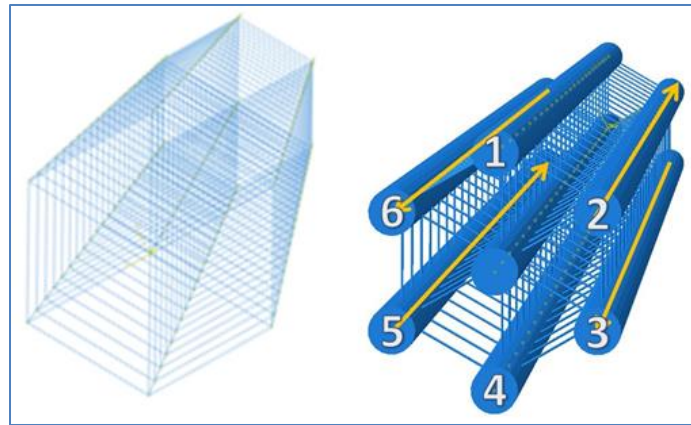
Figure 1. Previous finite element models of flagella.
(Left) Wireframe structure of the model.
(Right) Rendered model. Distributed axial loads are applied on coupled beams 2, 3, 5, 6
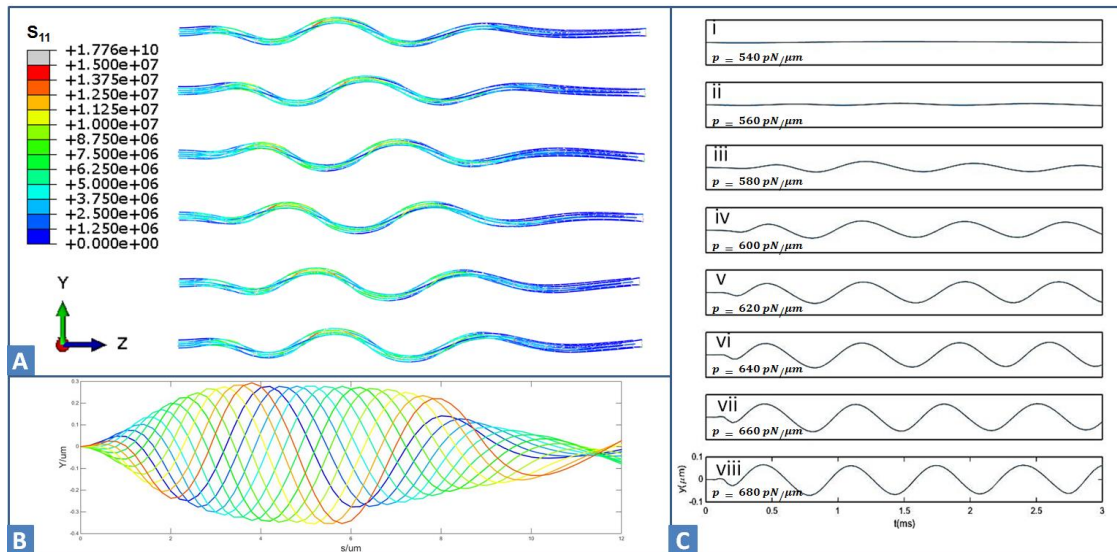
Figure 2. Wavelike oscillations in previous models. **(A)** Snapshots at six evenly spaced phases during one period of oscillation. **(B)** Time marching waveforms over one period of oscillation. **(C)** Displacement in y-direction at midpoint with steady, uniformly distributed dynein load of increasing magnitude.

However, the previous models are intentionally simplified to isolate instability and reduce computational cost – they have inevitable limitations.

A global mesh was applied on the entire model, and each inter-doublet link was meshed into two elements – such a coarse mesh resulted in inaccurate simulation. Therefore, in **Section 2.3**, re-seeding and re-meshing processes were performed on the old models to achieve a finer mesh and get more accurate results.

All beams were welded together – displacement and rotation were restricted with a preset relative tolerance of 1e-14 (**2**), which did not represent the actual structure of flagella well. As discussed in **Section 2.4**, new models use different connectors to represent inter-doublet flagella behavior.

All beams were purely elastic, neither viscoelasticity nor hyperelasticity were included as part of the material property, thus the simulation did not take them into consideration. In **Section 2.5**, new models introduce viscoelasticity of inter-doublet components.

Material properties of inter-doublet components were estimated. Plus, higher modulus was used to compensate for the missing hyperelasticity; there was no guarantee that the model shows similar realistic behavior of flagella. Nondimensionalization (**Section 2.6**) can be used to calculate new material properties given adjusted parameters, and the non-dimensional waveform will remain unchanged.

2   Modeling

2.1   Model Revisit

The structure of cilia and flagella is well-known: the underlying cytoskeleton, known as the "9+2" axoneme, consists of 9 slender, microtubule doublets (resembling elastic beams), arranged in a circular array about a central pair of 2 microtubules. These beam-like components are connected by radial spokes and circumferential nexin links, and driven by the motor proteins dynein.

In the viscoelastic flutter model (**3**), dynein activity is modeled as opposing steady, distributed tangential forces acting on coupled doublets (**Fig. 3**). Outer doublets are numbered from 1 through 9. Doublet 1, 5 and 6 are modeled as idle doublets which do not experience any force or torque. Doublet 2&3, 3&4, 7&8, and 8&9 are coupled doublets where the dynein force drives doublet N+1 tip-ward relative to doublet N.
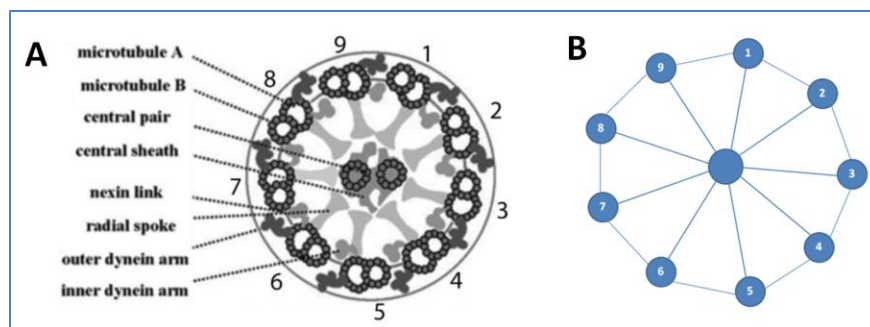

Figure 3. (A) Schematic diagram of cross-section of the flagellar axoneme showing key components: outer doublets (numbered clockwise from 1 through 9), a central pair, nexin links and dynein arms. **(B)** Simplified cross-sectional frame of a flagella.

To capture the oscillatory feature of the entire model, the cytoskeletal structure is simplified to minimize computational cost (**Fig. 3**): doublet 5 and doublet 6 are combined as one doublet since both are idle doublets; doublet 3 and doublet 8 are excluded since they experience both base-ward and tip-ward dynein forces; the central pair is treated the same as outer doublets. Material properties and geometric parameters of this baseline model are summarized in **Table 1**.

Table 1. Summary of key parameter values of the baseline model

Parameter	Value for 6-doublet model	Units	Description
N	6	Nondim.	Number of doublets
L_d	12	μm	Length of doublet
r_d	0.02	μm	Cross-sectional radius of doublet
E_d	8×10^8	Pa (pN/μm^2)	Young's modulus of doublet
v_d	0.4	Nondim.	Poisson's ratio of doublet
d	0.5	μm	Separation between each cross-section
a_s	0.1	μm	Length of spoke
r_s	0.001118	μm	Cross-sectional radius of spoke
E_s	4×10^{10}	Pa (pN/μm^2)	Young's modulus of spoke
v_s	0.4	Nondim.	Poisson's ratio of spoke
a_n	0.1	μm	Length of nexin link
r_n	0.001118	μm	Cross-sectional radius of nexin link
E_n	4×10^8	Pa (pN/μm^2)	Young's modulus of nexin link
v_n	0.4	Nondim.	Poisson's ratio of nexin link
D(s)	1 or $1-e^{s/s0}$	Nondim.	distribution of dynein force
α	73766	Nondim.	Mass proportional Rayleigh damping coefficient (all)
ρ	1×10^{-4}	pN-s^2/μm^4	Density (all)*

2.2 Re-meshing

In ABAQUS, by default, integration points in the same part are connected by weld joint. As a result, the baseline model was constructed as a single part so that all connections were weld. However, in ABAQUS, only a global algorithm can be selected as a single-part-model, therefore the mesh size is larger the size of inter-doublet beams, resulting in a coarse mesh on inter-doublet beams. As shown in **Fig. 4A**, each inter-doublet beam was meshed into one element, which led to inaccurate simulation result.
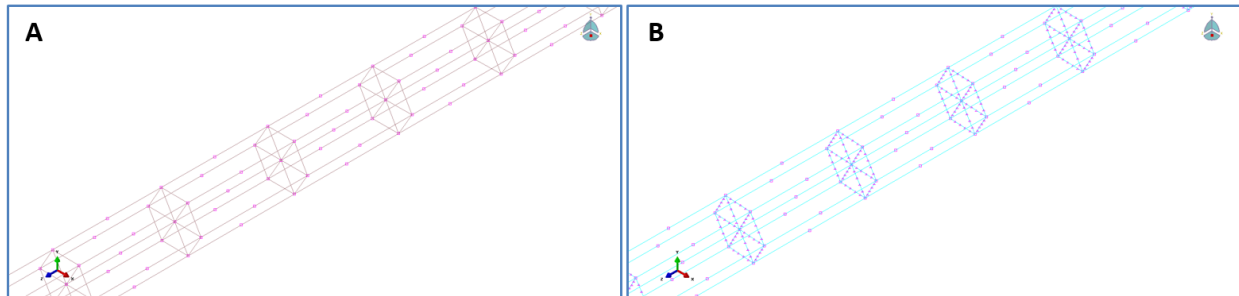

Figure 4. Seed and mesh setting for **(A)** baseline model. **(B)** new model.

To improve the coarse mesh setting on inter-doublet beams, the flagella model has to be separated into multiple parts. A part separation process was performed on the flagella model, and the model has been divided into three modules: doublet, nexin links, and radial spokes.

Each module was copied with a linear pattern to construct a flagella model with the same geometry as the baseline model, and same boundary conditions and loads were applied. In ABAQUS, when the assembly contains more than one part, local seeding algorithms can be modified, and a finer mesh was created for inter-doublet components (radial spokes and nexin links) with a seed size of 0.02. **Fig. 4B** shows the resulting finer seeding setting.

2.3 Multibody Dynamics

All joints in the baseline model are weld. In ABAQUS, connection type WELD provides a fully bonded connection between two nodes (**Fig. 5**).
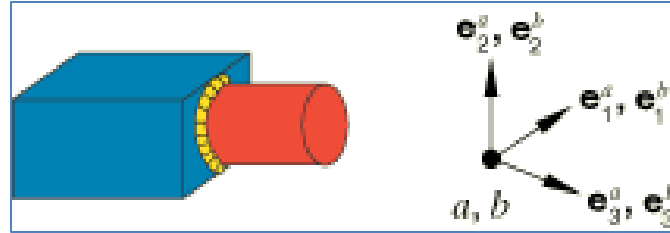

Figure 5. Schematic of connection type WELD

Displacement in all translational and rotational directions are constrained in a joint type WELD, which is not the case in real flagella. It is believed that radial spokes and circumferential nexin links have one end anchored at the doublet, and the other end climbing – sliding back and forth periodically. Since translation along the longitudinal direction of doublets and central pair was restricted in the baseline model, the sliding mechanism of inter-doublet components was completed ignored.

A different joint type TRANSLATOR is used in the new model. Connection type TRANSLATOR provides a slot constraint between two nodes and aligns their local directions (**Fig. 6**).
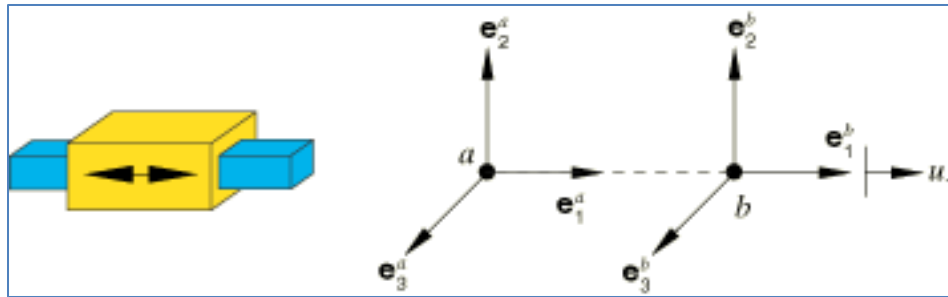
Figure 6. Schematic of connection type TRANSLATOR

Predefined Coulomb-like friction in the TRANSLATOR connection relates the kinematic constraint forces and moments in the connector to friction force in the translation along the slot (**4**). The frictional effect is formally written as

$$\Phi = P(f) - \mu F_N \leq 0 \tag{1}$$

where the potential $P(f)$ represents the magnitude of the frictional tangential traction in the connector in the local 1-direction, F_N is the friction-producing normal (contact) force in the direction normal to the slot, and μ is the friction coefficient. Frictional stick occurs if $\Phi < 0$; and sliding occurs if $\Phi = 0$, in which case the friction force is μF_N.

4

Fig. 7 shows the new model configuration after using TRANSLATOR as connection type between inter-doublet beam and outer doublet beam. For radial spokes, they are welded onto the outer doublet and sliding along the central pair. For nexin links, they are welded onto the N_{th} outer doublet and sliding along the $(N + 1)_{th}$ outer doublet.
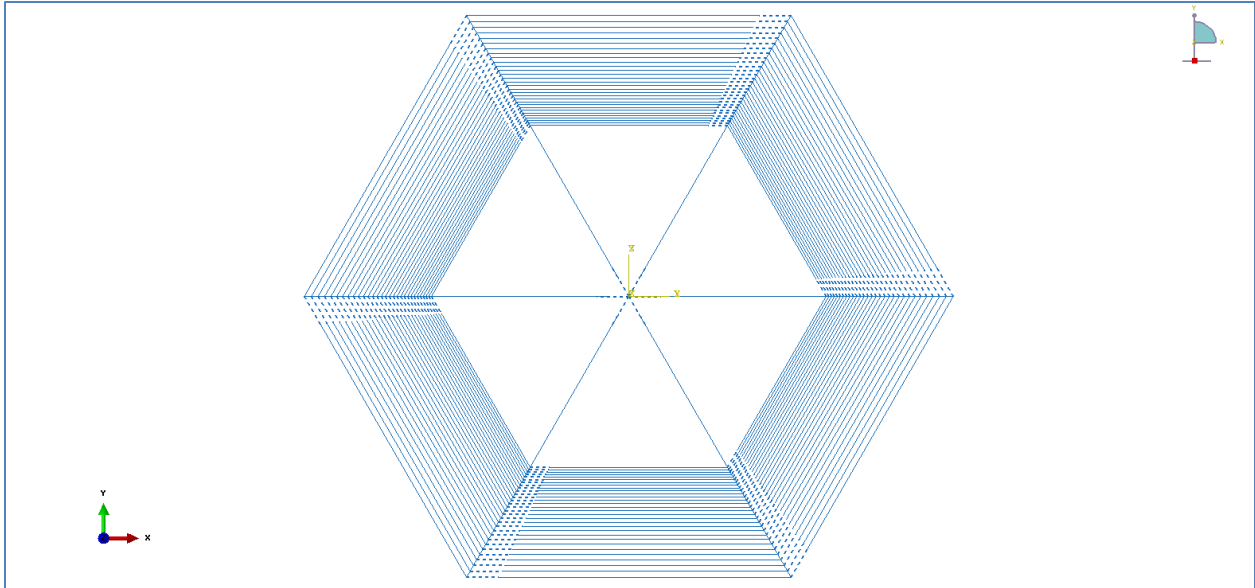
Figure 7. Wireframe structure of the new model with dash lines representing connection type TRANSLATOR

2.4   Viscoelasticity

The baseline model is purely elastic, and therefore viscoelastic behavior of inter-doublet components was not taken into consideration in simulation. However, creep and relaxation are important factors of modeling viscoelastic materials. When subjected to a step constant stress, viscoelastic materials experience a time-dependent increase in strain (**Fig. 8**). At time t_0, a viscoelastic material is loaded with a constant stress that is maintained for a sufficiently long time period. The material responds to the stress with a strain that increases until the material ultimately fails. When the stress is maintained for a shorter time period, the material undergoes an initial strain until a time t_1 at which the stress is relieved, at which time the strain immediately decreases (discontinuity) then continues decreasing gradually to a residual strain.

Figure 8. (Left) Applied stress and **(Right)** Induced strain as functions of time for a viscoelastic material

ABAQUS assumes that the time domain viscoelasticity is defined by a Prony series expansion (**5**). Viscoelasticity of inter-doublet components has been defined by Prony creep model, with $\bar{g}_i^P = 0.5$ shear relaxation or shear traction relaxation modulus, and $\tau_i = 0.01$ relaxation time constant.

2.5 Nondimensionalization

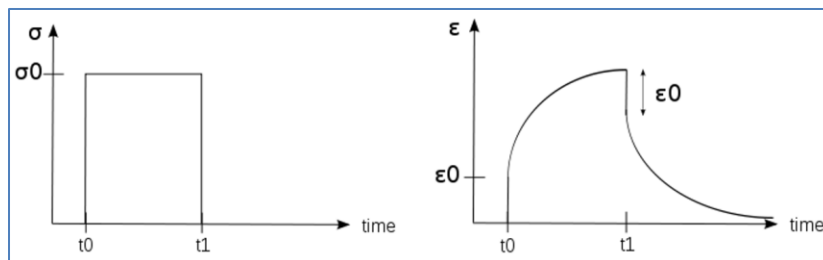Stability analysis of the linearized one dimensional (1D) partial differential equation (PDE) raised by Bayly and Dutcher (**6**) describes small-amplitude motion about a straight, equilibrium configuration. In the viscoelastic flutter model of flagella, the baseline tension (or compression) in the two doublets is:

Doublet 1: $T_{10} = p(L - s)$ (tension)

Doublet 2: $T_{20} = -T_{10}$ (compression)

Beam equation of the coupled doublets:

$$EI\psi_{1,ssss} - \frac{\partial}{\partial s}\left(p(L-s)\psi_{1,s}\right) + c_N\psi_{1,t} = -m_{,ss} - k_N(\psi_1 - \psi_2) - b_N(\psi_{1,t} - \psi_{2,t}) \qquad \textbf{(2)}$$

$$EI\psi_{2,ssss} + \frac{\partial}{\partial s}\left(p(L-s)\psi_{2,s}\right) + c_N\psi_{2,t} = -m_{,ss} + k_N(\psi_1 - \psi_2) + b_N(\psi_{1,t} - \psi_{2,t}) \qquad \textbf{(3)}$$

$$m = -k_T a^2 \bar{\psi} - b_T a^2 \bar{\psi}_{,t} \qquad \textbf{(4)}$$

, where E is the Young's modulus of each doublet $[Pa]$, I is the area moment of inertia about the longitudinal direction of the doublet $[m^4]$, p is the distributed dynein load $[pN/\mu m]$, L is the total length of the doublet $[\mu m]$, m is the mass of doublet $[pN \cdot s^2/\mu m]$, k_N is the interdoublet normal stiffness $[pN/\mu m^2]$, and b_N is the interdoublet normal viscous resistance. Following references (**7, 8, 9, 10, 11**) separable solutions of the form

$$\psi_n(s,t) = \exp(\sigma t)\tilde{\psi}_n(s) \qquad\qquad n = 1,2 \qquad \textbf{(5)}$$

are sought. After defining a characteristic time for the system, $\tau = c_N L^4/EI$, and a normalized eigenvalue, $\bar{\sigma} = \sigma\tau$, the resulting ordinary differential equations (ODEs) may be written in non-dimensional form:

$$\tilde{\psi}_1'''' - \bar{p}[(1-\bar{s})\bar{\psi}_1']' + \bar{\sigma}\bar{\psi}_1 = \bar{c}(\bar{\sigma})(\bar{\psi}_1'' + \bar{\psi}_2'') - \bar{d}(\bar{\sigma})(\bar{\psi}_1 - \bar{\psi}_2) \qquad \textbf{(6)}$$

$$\tilde{\psi}_2'''' - \bar{p}[(1-\bar{s})\bar{\psi}_2']' + \bar{\sigma}\bar{\psi}_2 = \bar{c}(\bar{\sigma})(\bar{\psi}_1'' + \bar{\psi}_2'') + \bar{d}(\bar{\sigma})(\bar{\psi}_1 - \bar{\psi}_2) \qquad \textbf{(7)}$$

, where the new non-dimensional parameters are $\bar{p} = pL^3/EI$, $\bar{c}(\bar{\sigma}) = (k_T a^2 + b_T a^2 \bar{\sigma})L^2/EI$, and $\bar{d}(\bar{\sigma}) = (k_N + b_N\bar{\sigma})L^2/EI$.

To maintain the waveform, natural frequencies, and forced frequencies of the model, non-dimensionalized **Eq. 6 and 7** MUST hold at all times. In other words, non-dimensional parameters should remain unchanged:

$$\bar{p} = pL^3/EI \qquad \textbf{(8)}$$

$$\bar{c}(\bar{\sigma}) = (k_T a^2 + b_T a^2 \bar{\sigma})L^2/EI \qquad \textbf{(9)}$$

$$\bar{d}(\bar{\sigma}) = (k_N + b_N\bar{\sigma})L^2/EI \qquad \textbf{(10)}$$

, where $\bar{p}$ is the non-dimensional distributed load, $\bar{c}$ is the non-dimensional tangential resistance, and $\bar{d}$ is the non-dimensional normal resistance.

Non-dimensional parameters can be further simplified by substituting in material properties of spokes and nexin links, and because the flexural rigidity EI of doublets have been measured experimentally with a high accuracy (**12**), we would like to keep EI unchanged as well:

$$\bar{p}EI = pL^3 \tag{11}$$

$$\bar{c}EI = k_T a^2 L^2 = \frac{\left(\frac{3E_s I_s}{L_s^3} + \frac{3E_n I_n}{L_n^3}\right)a^2 L^2}{d_c} = \left(\frac{3I_s a^2}{L_s^3 d_c}\right)\left(E_s + \frac{I_n L_s^3}{I_s L_n^3}E_n\right)L^2 \tag{12}$$

$$\bar{d}EI = k_N L^2 = \frac{\left(\frac{E_s A_s}{L_s} + \frac{E_n A_n}{L_n}\right)L^2}{d_c} = \left(\frac{A_s}{L_s d_c}\right)\left(E_s + \frac{A_n L_s}{A_s L_n}E_n\right)L^2 \tag{13}$$

, where E_s and E_n are Young's moduli of spoke and nexin link, I_s and I_n are area moment of inertia of spoke and nexin link, L_s and L_n are length of spoke and nexin link, respectively, and d_c is the separation between cross-sections along the longitudinal direction of doublet.

2.6 Optimization

Nondimensionalization can also be used to reduce computational cost. Here I would like to propose a way to minimize computational cost by constraining the nondimensional waveform unchanged and adjusting geometric and load parameters. The cost function should be in a similar form as follows:

$$\min_{p,L,E_s,E_n>0} f(p,L,E_s,E_n) \tag{O}$$

$$Subject\ to:$$

$$pL^3 = 933120 \tag{C1}$$

$$(E_s + E_n)L^2 = 5.8176 \times 10^{12} \tag{C2}$$

$$\frac{pL}{E_s + E_n} \leq 1.96 \times 10^{-7} \tag{C3}$$

where constraints **C1** and **C2** result from nondimensional **Eq. 11-13**, and constraint C3 results from stability constraint. Assuming the cost function $f(p,L,E_s,E_n)$ is a linear combination of cost functions of each parameter, and is in the form of

$$cost = Ap + BL + CE_s + DE_n + E = -(2.72 \times 10^{-4})p + (3.98 \times 10^{-2})L + (3.41 \times 10^{-12})E_s + (4.67 \times 10^{-10})E_n \tag{14}$$

By using optimum parameter values that minimize the cost function **Eq. 14**, simulation time can be reduced.

3   Results

Simulation results of four representative models are displayed below. **Table 2** summarizes and compares key parameter values of each model, **Fig. 9** shows time-marching waveforms of each model.

Table 2. Summary of key parameter values of four representative models

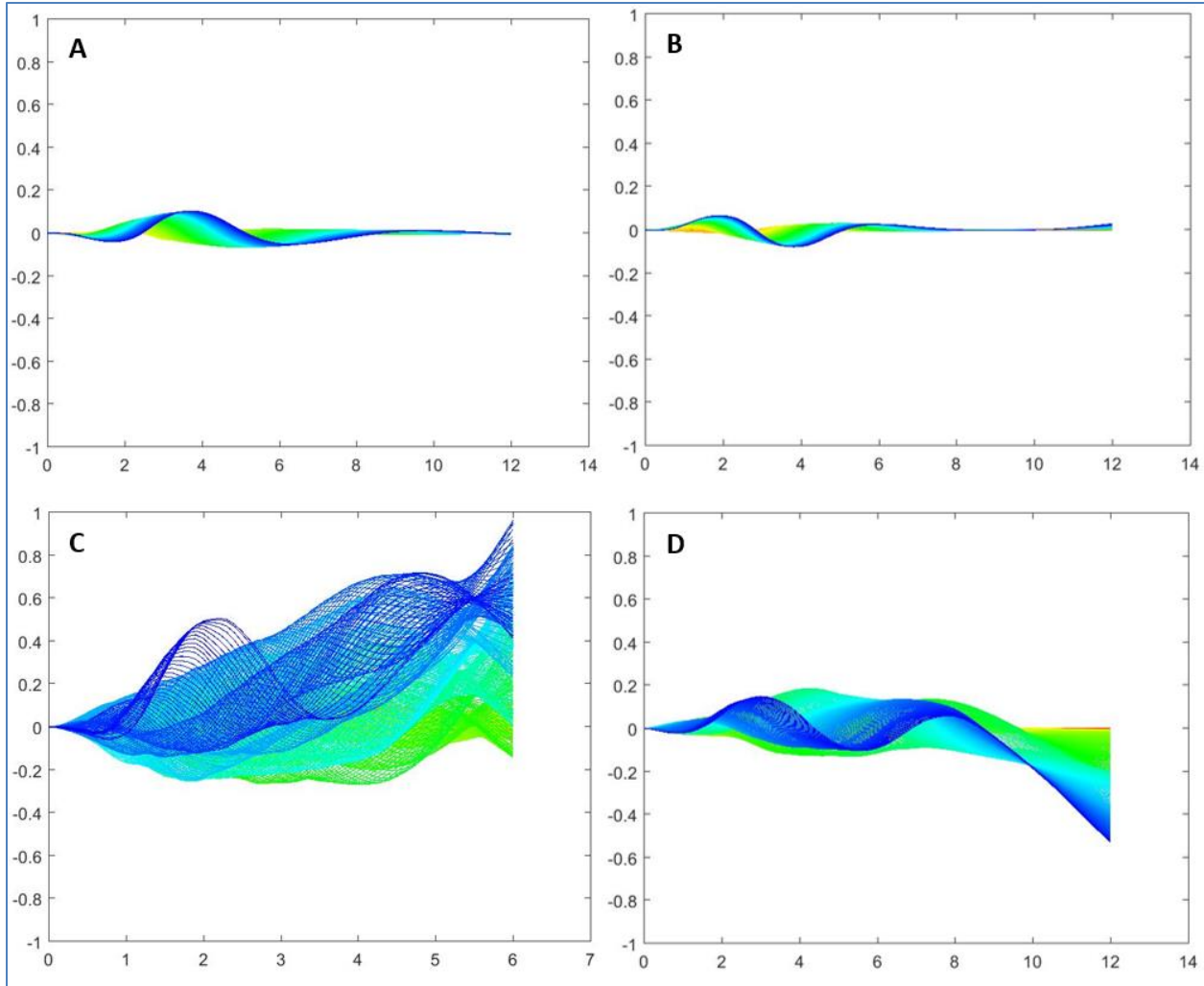|	Baseline model 1	Baseline model 2	New model 1	New model 2
Number of doublets	6	6	6	6
Length of doublet	12	12	6	12
Radius of doublet	0.02	0.02	0.02	0.02
Young's modulus of doublet	8E8	8E8	8E8	8E8
Poisson's ratio of doublet	0.4	0.4	0.4	0.4
Rayleigh damping	73766	73766	73766	73766
Mesh size of doublet	0.2	0.2	0.2	0.2
Longitudinal separation	0.4	0.4	0.4	0.4
Length of spoke	0.1	0.1	0.09	0.09
Radius of spoke	0.0001118	0.0001118	0.0001118	0.0001118
Young's modulus of spoke	4E10	4E10	8E10	2E10
Poisson's ratio of spoke	0.4	0.4	0.4	0.4
Shear relaxation modulus ratio of spoke	NA	NA	0.5	0.5
Relaxation time constant of spoke	NA	NA	0.01	0.01
Connector type at central pair	WELD	WELD	TRANSLATOR	TRANSLATOR
Friction coefficient of spoke	NA	NA	0.5	0.5
Mesh size of spoke	0.1	0.1	0.01	0.01
Length of nexin	0.1	0.1	0.09	0.09
Radius of nexin link	0.0001118	0.0001118	0.0001118	0.0001118
Young's modulus of nexin link	4E8	4E8	4E8	1E8
Poisson's ratio of nexin link	0.4	0.4	0.4	0.4
Shear relaxation modulus ratio of nexin link	NA	NA	0.5	0.5
Relaxation time constant of nexin link	NA	NA	0.01	0.01
Connector type at lower doublet	WELD	WELD	TRANSLATOR	TRANSLATOR
Friction coefficient of nexin link	NA	NA	0.5	0.5
Mesh size of nexin link	0.1	0.1	0.01	0.01
Load distribution	Distally increasing	Distally increasing	Distally increasing	Distally increasing
Load magnitude	540	600	2500	312.5

Figure 9. Four time marching waveform plots (Red → Blue corresponds to Initial → End) of **(A)** baseline model 1 **(B)** baseline model 2 **(C)** new model 1 **(D)** new model 2.

4 Discussion and Conclusion

Baseline models 1 and 2 are models developed previously with different load magnitudes (**Fig. 9A-B**). New models 1 and 2 are improved models using MBD joints and with viscoelasticity included (**Fig. 9C-D**). Since the new models use connector type TRANSLATOR to represent sliding radial spokes and nexin links, their resulting waveforms have larger deflections than baseline models.

According to **Eq. 11-13**, new model 1 and new model 2 have same nondimensional load and resistive coefficients, therefore they should have similar waveforms. However, it is observed that their waveforms differ noticeably. Errors might have come from assumptions made in deriving nondimensional equations.

Current models show waves at frequencies much higher than practical values of real flagella. Future work involves using Nondimensionalization to find the parameter values resulting in frequencies in the right range.

References

1. Hu T., Dutcher, S. K., and Bayly, P. V., "Dynamic Instability and Wavelike Oscillations in A 9-doublet Finite Element Model of Flagella" (2016), IMECE 2016-68778.

2. "Understanding contact and constraint detection," Abaqus documentation, Abaqus/CAE User's Guide Section 15.6.

3. Bayly P. V., Wilson K.S., "Equations of Interdoublet Separation during Flagella Motion Reveal Mechanisms of Wave Propagation and Instability,"(2014) *Biophysical Journal*;107(7):1756-1772. doi:10.1016/j.bpj.2014.07.064, p. 1758.

4. "Understanding connector sections and functions," Abaqus documentation, Abaqus/CAE User's Guide Section 15.8.

5. "Defining time domain viscoelasticity," Abaqus documentation, Abaqus/CAE User's Guide Section 12.9.1.

6. Bayly, P. V., Dutcher, S. K., "Steady dynein forces induce flutter instability and propagating waves in mathematical models of flagella," (2016), *Biophysical Journal.*

7. Riedel-Kruse I.H., Hilfinger A., Howard J., & Julicher F. (2007) How molecular motors shape the flagellar beat. HFSP J 1(3):192-208.

8. Hilfinger A., Chattopadhyay A.K., & Julicher F. (2009) Nonlinear dynamics of cilia and flagella. Phys Rev E Stat Nonlin Soft Matter Phys 79(5 Pt 1):051918.

9. Camalet S. & Julicher F. (2000) Generic aspects of axonemal beating. New J Phys 2:241-2423.

10. Bayly P.V. & Wilson K.S. (2014) Equations of inter-doublet separation during flagella motion reveal mechanisms of wave propagation and instability Biophys J 107(7):1756-1772.

11. Bayly P.V. & Wilson K.S. (2015) Analysis of unstable modes distinguishes mathematical models of flagellar motion. Journal of the Royal Society, Interface / the Royal Society 12(106).

12. G. Xu, K.S. Wilson, R.J. Okamoto, J.Y. Shao, S.K. Dutcher, P.V. Bayly. Flexural rigidity and shear stiffness of flagella estimated from induced bends and counterbends. Biophysical Journal. 110(12):2759-68. 2016. PMID: 27332134.